Rydberg states about dipolar cores: The quantum dynamics of the long-range anisotropic interaction

L. Ya Baranov
The Fritz Haber Research Center for Molecular Dynamics, The Hebrew University, Jerusalem 91904, Israel

F. Remacle
Département de Chimie, B6, Université de Liège, B-4000 Liège, Belgium

R. D. Levine*
The Fritz Haber Research Center for Molecular Dynamics, The Hebrew University, Jerusalem 91904, Israel

(Received 21 March 1996; revised manuscript received 14 June 1996)

High Rydberg states about a dipolar molecular core can exhibit special features due to the exceptionally long range of the electrical anisotropy of the core. Unlike all other, more localized, couplings of the Rydberg electron to the ion, here the interaction is not shielded by the centrifugal barrier. The influence of the core even on states of the electron with higher angular momentum l and the significant matrix elements between states that differ considerably in the principal quantum number n make this problem worthy of separate considerations. Using specialized computational techniques (both analytical and numerical) for the exact evaluation of the relevant matrix elements, the role of both inter- and intra-Rydberg series coupling is discussed. The importance of the latter (i.e., the coupling of the Rydberg electron to the rotation of the core) is emphasized. Special attention is given to the role of an external dc electrical field that is different in the present problem in that it does not significantly dilute the strength of the electron-core interaction. A positively charged core can have a dipole moment (defined with respect to its center of mass) larger than that of neutral polar molecules, particularly if the charge is localized. Hence the interseries and intraseries dynamics discussed in this paper can give rise to experimentally measurable special effects. [S1050-2947(96)01112-2]

PACS number(s): 31.15.−p, 33.80.Rv, 03.65.Ge, 34.50.Gb

I. INTRODUCTION

The power of selective pulsed field ionization of high Rydberg states for providing high-resolution spectra of molecular and cluster ions has recently been demonstrated [1–9]. In addition, by varying the delay of the ionizing pulse, time-resolved studies, from several nanoseconds to many microseconds, can be achieved [9–13]. The initially excited state can undergo complex, multi-time-scale dynamics during such intervals that are very long compared to the (itself long) orbital period of the Rydberg electron [14]. The rather weak couplings that can be important over such long times also mean that the role of external perturbations, which are otherwise often of marginal importance, need to be examined [12,13,15–26].

In this paper we consider the special features that are to be expected for molecular Rydberg states when the central ionic core has a dipolar anisotropy. The range of such an interaction r^{-2} (where r is the distance from the electron to the center of mass of the core) is comparable to that of the centrifugal barrier in the orbital motion of the electron. Unlike the case of more localized electron-core couplings, the centrifugal barrier is far less effective in shielding the electron from the dipolar anisotropy. Electrons with angular momentum l as high as, roughly, $0.5n$ can still be coupled. In particular, this means that a dc electric field does not act so as to significantly reduce the electron-core coupling by inducing mixing of l states. A not so intuitively obvious feature of the long-range potential is that it can preferentially and effectively couple orbitals with rather different values of n. This is particularly expressed when we consider interseries couplings, that is, changes in n accompanied by changes in the rotational state j of the core.

The numerical results that we present are obtained by an exact diagonalization of the Hamiltonian using a zeroth-order basis spanning a finite-energy band. Two alternative zeroth-order bases are used to describe the orbital motion of the electron. One is the familiar hydrogenic one. For this case, an external dc electrical field, if present, must be treated as part of the perturbation. The alternative, discussed in Sec. IV, is to include the dc field as part of the zeroth-order description.

The discussion of the results is based on the properties of the matrix elements of the coupling between the zeroth-order states of the electron. It is therefore important that these matrix elements are correctly evaluated, particularly so since we argue that large changes in quantum numbers are possible. Analytical and numerical results are presented to support the conclusions. The Appendix provides a detailed discussion of the recursion procedure that we use. This method has been validated against analytical results (when the agreement is within the accuracy of the computer) and also using wave functions generated by Numerov integration [27–30] and the two sets of numerical results agree to within 1%. The importance of large changes in the quantum numbers and the range of the coupling being comparable to the centrifugal barrier

*Author to whom correspondence should be addressed. Fax: 972-2-6513742. Electronic address: rafi@batata.fh.huji.ac.il

mean that the near-threshold Bessel approximation for the radial wave functions of high n [31] is not sufficient even on qualitative grounds. The numerical procedures discussed in the Appendix of this paper are not limited to a dipolar coupling and have also been used to generate the Stark matrix elements needed below and also for the quadrupolar anisotropy, which is discussed in detail elsewhere.

The special features of the dipolar matrix elements imply that this coupling is not important for low and intermediate molecular Rydberg states. The reason is the Δn dependence of the coupling, which is weak in the $\Delta n \ll n$ limit. Detailed results demonstrating this effect are provided in Secs. II and IV below. When n is low, the most nearly isoenergetic state of another series has n' comparable to n. This is the Born-Oppenheimer regime. The interseries dipolar coupling is important precisely in the higher-n regime, which is being currently explored by ZEKE (zero electron kinetic energy) spectroscopy.

Besides the special feature expected for the dipolar coupling, there is another reason for our interest. It is likely that this coupling is stronger and more common than one might expect on the basis of the magnitude of typical dipoles of neutral polar molecules. The point is that, for ZEKE spectroscopy of neutral parents, the dipole in question is the dipole of the positively charged core about which the Rydberg electron revolves. Unless the core is homonuclear, this dipole, which is defined with respect to the center of mass (and not the center of charge) of the core, can be of the order of more than 1 a.u. This will be particularly the case for polyatomic molecules that contain a side group where the charge will be localized.

The theoretical interest in dipolar coupling is about as old as the interest in autoionization of molecules [32–38]. The present work differs in several respects from the earlier studies. One practical difference is that we are primarily interested in high-n Rydberg states. It is then reasonable to use a zeroth-order basis, where each rotational state of the core has its own series of Rydberg states, rather than the use of a Born-Oppenheimer basis. Within that basis we compute matrix elements using exact radial wave functions (rather than using a Bessel approximation) and diagonalize the Hamiltonian within a band of quasi-isoenergetic states. An important point about the zeroth-order basis is that it contains more than one series (i.e., more than one rotational state of the core) so that we examine both intra- and interseries coupling. We also include the intraseries n and l Stark mixing due to an external dc field. As we shall point out in detail below, each one of these seemingly technical points has qualitative implications for the dynamics. Two conclusions that are important enough to note are in particular the following. (i) The role of the dc field is not primarily to dilute the coupling strength [15,23,39–41]. Dilution is important for all the other, more localized, electron-core interaction and even the r^{-3} quadrupolar coupling is qualitatively different from the dipolar one [42]. (ii) The (interseries) coupling of the electron to the rotation of the core is not negligible.

Section II examines the matrix elements of the dipolar interaction. The rest of the paper hinges upon the two main qualitative results of this section. (i) The matrix elements do not necessarily decline as the orbital angular momentum of the electron increases. Indeed, on the average, the coupling strength is roughly constant up to l/n of about 0.3. (ii) While the coupling is strictly zero if $n=n'$ and is very small when $n-n'$ is small, as $n-n'$ increases the coupling increases both in the hydrogenic and in the parabolic zeroth-order states. In the hydrogenic basis, the coupling reaches a plateau and then finally decreases. The height of the plateau is higher for lower l and the value of n' for which it is reached decreases with l. On the other hand, in the parabolic states, there is a monotonic increase as n' decreases and the magnitude of the coupling is smaller for lower $|k|$ parabolic states. In both zeroth-order bases, the dipolar coupling takes significant values for finite $n-n'$ values. The simpler problem of intraseries coupling is discussed in Sec. III and the behavior of the dipolar coupling in parabolic states in Sec. IV. Section V discusses the implications for the importance of inter series coupling and for the role of an external dc field. Particular attention is given to the case when the field is above the Inglis-Teller limit [30]. This is the limit when the Stark manifold of states of different n's begin to overlap so that the density of states reaches its uniform value n^4 (in a.u.). The n^{-5} scaling of this onset means that it occurs at quite low fields for high Rydberg states. Numerical results for the temporal evolution are given in Sec. VI. Conclusions are given in Sec. VII. The Appendix provides the details of the two versions of the recursion method used to generate accurate matrix elements when n and also l are high.

II. RADIAL MATRIX ELEMENTS OF THE DIPOLAR COUPLING

The selection rules for the dipolar coupling, determined by the angular part of the interaction, imply that radial matrix elements are only required for changes of l of ± 1. These selection rules are identical for those for absorption of light as can be seen from the so-called acceleration form of the radiative matrix elements [43]. For a hydrogenic electron $H_0=\mathbf{p}^2/2-1/r$ of position and momentum $\mathbf{r}$ and $\mathbf{p}$

$$\mathbf{r}/r^3=-i[H_0,\mathbf{p}]=[H_0,[H_0,\mathbf{r}]], \tag{1}$$

where the square bracket denotes the commutator. Taking matrix elements of both sides,

$$\langle n'l'm'|\mathbf{d}\cdot\mathbf{r}/r^3|nlm\rangle=\tfrac{1}{4}(n'^{-2}-n^{-2})^2\langle n'l'm'|\mathbf{d}\cdot\mathbf{r}|nlm\rangle, \tag{2}$$

where $\mathbf{d}$ is the dipole moment of the core. When the coupling of the electron is to a molecular core, the selection rule for m is that for either change in $l, \Delta m=0,\pm 1$. The identity also shows the long-range nature of the dipolar coupling and the wide range of n's that can be coupled.

The matrix elements are, as usual [44–46], expressed as a product of a radial and an angular term

$$\langle n'l'm'|\mathbf{d}\cdot\mathbf{r}/r^3|nlm\rangle=d\langle n'l'|1/r^2|nl\rangle\cdot\langle l'm'|\hat{\mathbf{d}}\cdot\hat{\mathbf{r}}|lm\rangle, \tag{3}$$

where the caret denotes the unit vector. The angular terms are standard analytical integrals [43], but note that the m dependence is such that the $\Delta m=\pm 1$ terms are about a factor of 2 smaller than the $\Delta m=0$ ones. Since the total M is conserved, the changes in m of the electron are compensated by corresponding changes in the orientation quantum number of

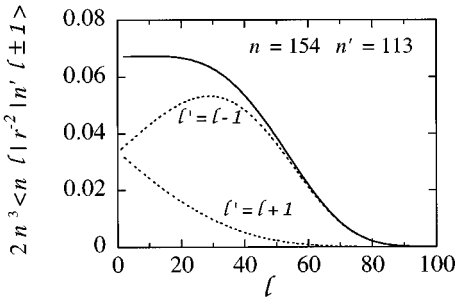

FIG. 1. Matrix elements of the dipolar coupling between $n=154$ and $n'=113$ vs l computed by the recursion method discussed in the Appendix. The matrix elements are shown multiplied by $\rho=n^3$, the density of states in the absence of an external electrical dc field. The reason for this choice is that the dimensionless parameter $\gamma=2V\rho$ is discussed in Sec. V as the measure of the average coupling strength in the absence of an external field. Shown are the two possible transitions corresponding to $l'=l\pm1$ (dots) and the sum of the two matrix elements (solid line). Note the very wide range in l over which the coupling extends.

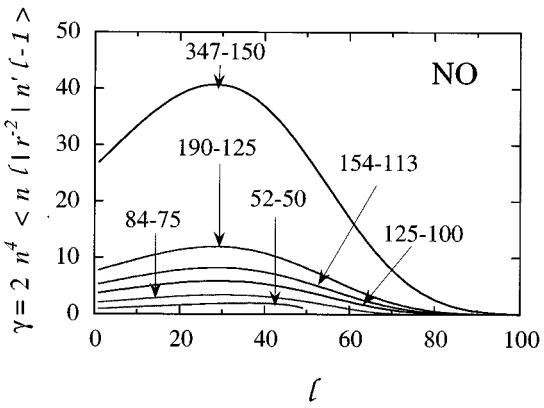

FIG. 2. Matrix elements of the dipolar coupling between pairs of states of different n's in NO vs l. The states chosen are all about isoenergetic when they belong to two different series built upon the $j=0$ and 1 rotational states of NO^+ ($B=1.9842\ cm^{-1}$). The matrix elements are shown multiplied by the density of states $\rho=n^4$ in the presence of an electrical field. Note, however, that V is a product of the radial matrix element by an angular factor that is an expectation value of a cosine of an angle and hence this additional factor is below unity. Therefore Rydberg states of higher but not very high n's are not strongly coupled.

the core. This compensation is not possible when the coupling is due to an external dc field. A Stark mixing has strictly an intraseries character.

The experience with radiative matrix elements is that they require accurate radial wave functions for their evaluation [31]. The recursion procedure discussed in the Appendix was found to be very accurate. It was checked using analytical results for both diagonal and off-diagonal matrix elements. In particular, the identity [47]

$$[l(l+1)-l'(l'+1)]\langle n'l'|1/r^2|nl\rangle=(n'^{-2}-n^{-2})\langle n'l'|nl\rangle \tag{4}$$

was found useful for this purpose. As discussed in the Appendix, the recursion method was also compared with a purely numerical procedure using radial wave functions generated by a Numerov integration. Except at very high values of both n and l, where the recursion procedure is to be preferred, the two methods agree with the Numerov procedure being accurate to approximately 1%. The recursion method is very accurate, but inefficient, so that the Numerov method can be used as a practical alternative. See the Appendix for more details.

When the binding energy $(-1/2n^2)$ of the electron is small compared to the potential and/or the centrifugal energies, the radial wave function can be approximated as a Bessel function [31]. Approximate analytical expressions for the radial matrix elements derived using such Bessel radial wave functions were found not to be quite satisfactory. For large changes in the principal quantum number, these results are, as is to be expected, unreliable. Further details on the comparison are provided in the Appendix.

Figure 1 shows the dependence of the radial matrix elements on l for given n and n'. There are two possible transitions for a given $l,\Delta l=\pm1$. For $n-n'>0$, the $\Delta l\equiv l'-l=+1$ terms are smaller and decrease with l (Fig. 1). The $\Delta l=-1$ terms are bigger and initially increase with increasing l. The sum of the two terms is nearly constant up to $l/\min(n,n')$ of about 0.3 and decreases thereafter. The midpoint is at $l/\min(n,n')\simeq0.5$. The magnitude of the coupling is n dependent also because of the energy term in Eq. (2). In Fig. 1, the matrix elements are shown multiplied by n^3, the density of states ρ in the absence of an external dc field. The dimensionless parameter $2V\rho$ is discussed in Sec. V below and provides a measure of the average coupling strength. Figure 2 shows, vs l, the magnitude of the radial matrix elements for coupling of two nearly isoenergetic Rydberg states that belong to distinct series ($j=0$ and 1) in NO^+. Here the matrix elements are shown multiplied by n^4, the density of states (or quasi degeneracy) in the presence of a dc field.

The dependence of the radial matrix element on the change in the principal quantum number n is shown in Fig. 3. From the identity (4) the matrix element vanishes for $\Delta n=0$. The phase mismatch between radial wave functions of similar values of n lead to a matrix element that is small when Δn is small. However, as $n-n'$ increases, the radial matrix does reach significant values. The coupling reaches a plateau and then decreases as $\min(n,n')\rightarrow l$. The position of the plateau in n' occurs for larger values of Δn and its height is higher as l decreases. It is this variation that is not captured when the matrix element is approximated using the Bessel wave functions [48] that are otherwise realistic at very high n's. See Fig. 18 below for more details on this point.

The matrix element for Δn changes is relevant to both inter- and intraseries coupling. For a given series, the small value of the dipolar coupling for adjacent states means that its role will be small. Coupling of states of the same series that differ very much in their values of n is not important because these states will differ considerably in their energy. This is no longer true for coupling of states that belong to different series where the electronic energy mismatch can be made up by the difference in the rotational energy of the core. An additional reason why interseries dipolar coupling can be significant is that the large changes in n are possible for a wide range of values of l (cf. Fig. 2).

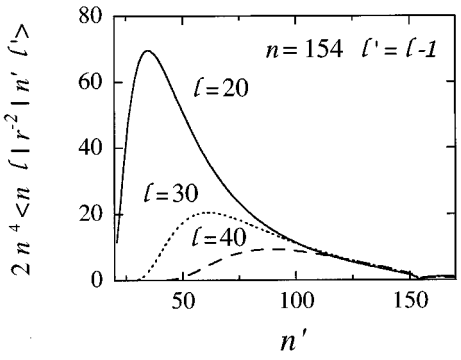

FIG. 3. Matrix elements of the dipolar coupling between a state of given $n=154$, $l=20$, 30, 40, and $l'=l-1$ vs n'. The matrix elements are shown multiplied by the density of states $\rho=n^4$ in the presence of an electrical field. Note the vanishing of the coupling for $n=n'$ and the low value when Δn is small. The peaking of the coupling for a fairly large value of Δn (which increases with decreasing values of l) means that two different Rydberg series corresponding to two different states of the core will experience different coupling strengths depending on the energy difference of the two states of the core and of n; cf. Fig. 2.

III. INTRASERIES DIPOLAR COUPLING

The coupling of Rydberg states for a given rotational state of the core has been studied by Zon [49] by averaging the Hamiltonian for the Rydberg electron

$$H=H_0+H_{\rm rot}+\mathbf{d}\cdot\mathbf{r}/r^3 \tag{5}$$

over the rotational state. Earlier studies [50,51] used a resting dipole. The eigenvalue problem for the Hamiltonian (5) in a given state of $H_{\rm rot}$ separates into an angular and radial parts. There is a problem for very low l's, a problem that has been recognized early on [33,34,38,52] in that states of very low l can penetrate too much into the core up to distances [53] where the approximation of the interaction in a multipole expansion is physically not realistic. Typically, for $l\geqslant 4$, the Hamiltonian (5) is realistic.

The model leads to a quantum-defect-like eigenvalue

$$E=-1/2(n_r+\lambda+1)^2, \tag{6}$$

where n_r is the radial quantum number and λ is an n_r independent noninteger parameter, which at high λ's is essentially l. This shows that, as expected on the basis of the radial matrix elements (Figs. 1 and 3), the intraseries dipolar coupling is limited, particularly so at higher λ's, and that for any but the lowest l's the states exhibit a single pure l character.

For the high n's of interest in this paper, an external dc electric field is typically above the Inglis-Teller limit $3n^5F$ (a.u.)$\geqslant 1$ [30] and can induce a more extensive mixing of the zeroth-order hydrogenic states not only in l (Stark splitting) but also in n. The role of the electric field is qualitatively similar to that expected in the absence of a dipole because above the Inglis-Teller limit the field matrix elements are, for ordinary dipoles (1 D=0.393 a.u.), bigger than the dipolar coupling (Fig. 4). The semiquantitative argument is as follows. The matrix element on the right-hand side of Eq. (2) is also that for Stark mixing of the hydrogenic states if we

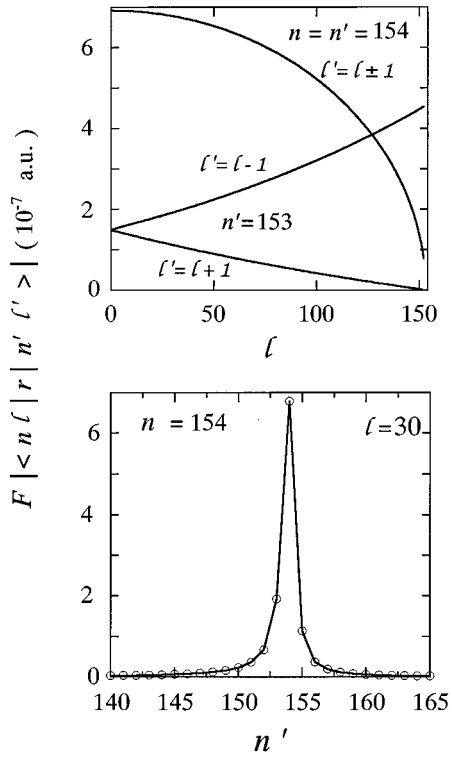

FIG. 4. Stark matrix elements ($\times 10^7$/a.u.) for a field of 0.1 V/cm, (a) as a function of l and (b) vs n. The Stark coupling, due to the external dc field, connects only zeroth-order states of the same Rydberg series. This is due to the conservation of M, the projection of the total angular momentum. On the other hand, for the dipolar coupling due to the core, the change in m_l can be compensated by a change in m_j so that interseries coupling is possible.

interpret **d** as the external dc field. Since the fore factor (the square of the energy difference) is of the order of $(\Delta n/n^3)$, it follows that the ratio of the internal dipolar coupling to the external field of magnitude F is $(\Delta n/n^3)^2 d/F$. If the field is above the Inglis-Teller limit, it follows that the field matrix element dominates. As emphasized in Fig. 4, the electric field couples not only states of given n but also mixes in adjacent Rydberg states.

In the computational examples we consider a diatomic ionic core in a Σ electronic state such as NO^+. The intraseries dipolar coupling is then absent and only the dc field can mix the zeroth-order states. When the electronic state of the core carries angular momentum or for a core that is a symmetric top, the coupling does not vanish. However, with or without the presence of an external dc field, the anisotropic coupling is not a major effect in the dynamics of high Rydberg states. Precisely because of the long-range nature of this interaction it acts, in a given series, as an additional contribution to the centrifugal term. Unless l is very low and/or the dipole is large [54–56], the effect is small. The physically important manifestations of the long-range interaction are in the interseries effects.

IV. DIPOLAR COUPLING IN PARABOLIC STATES

The field-induced (intraseries) coupling is often discussed [15,23,39,41] as the cause of lifetime elongation in high

Rydberg states. In a time-independent picture this is often termed a dilution effect: The field mixes low- and higher-l states so that the weight of low-l states in an eigenstate is, on the average, proportional to $1/n$. [We shall, however, note (cf. Fig. 5 below) that systematic and wide variations about the average are the rule.] In time-dependent language, the periodic modulation of l by the field means that the fraction of time that the system spends in low l's is reduced by a factor proportional to $1/n$ (see Fig. 16 below). The dipolar coupling, which is effective in the range $0 \leqslant l/n \leqslant 0.5$, will not, however, be significantly reduced by this depletion of the occupancy of the low-l states. It remains true that the field significantly reduces the fraction of time the system spends in low-l states, but the higher-l states can still be effectively coupled by the dipolar interaction.

The mixing of the dipolar coupling strength induced by an external dc field can be discussed using the zeroth-order parabolic [30,31] n,k,m states. The parabolic states correspond to the Stark eigenstates when the intraseries n mixing induced by the field is neglected. In this case, the Stark matrix elements are proportional to the strength of the field F and the Stark eigenstates are field-independent linear combination of the zeroth-order hydrogenic l states of common value n and m [30]. The relation between the parabolic states $|nkm\rangle$ and the hydrogenic states $|nlm\rangle$ is

$$|nkm\rangle = \sum_{l=0}^{n-1} \langle nlm|nkm\rangle |nlm\rangle, \tag{7}$$

where $\langle nkm|nlm\rangle$ are the $3j$ Clebsch-Gordan coefficients [30,57]. The weights in the l states of three parabolic k states differently localized in l are plotted in Fig. 5. In the upper panel plotted is the most localized in l, highest-k state $|k|=153$, which is localized up to $l=30$ in the region where the dipolar coupling in the l states is maximum (see Fig. 1). A parabolic state $|k|=135$ localized up to $l=l_0$, where $l_0 \approx 80$ is the range of the dipolar coupling in the l state basis, is shown in the middle panel and the most delocalized in l parabolic state $|k|=1$ (with a maximum in high l, but distributed over the whole range of l values) in the lower panel. Parabolic states k and $-k$ have the same distributions of weights.

In the parabolic states, the dipolar matrix elements take the form

$$\langle n'k'm'|r^{-2}|nkm\rangle = \sum_{l'=0}^{n'-1} \sum_{l=0}^{n-1} \langle n'k'm'|n'l'm'\rangle \times \langle n'l'm'|r^{-2}|nlm\rangle \langle nlm|nkm\rangle,$$

$$\delta_{ll'} = \pm 1, \delta_{mm'} = 0, \tag{8}$$

where $\langle nl|r^{-2}|n'l'\rangle$ are the matrix elements in the hydrogenic zeroth-order states plotted in Figs. 1–3. These matrix elements ($n=154$ and $n'=113$) are plotted in Fig. 6 as a function of k' for the three $n=154$ parabolic k states shown in Fig. 5. For a given value of k, the coupling is well localized within 5–8 values of k'. The value of k', k'_m that corresponds to the maximum is approximately given by $k'_m/k'_{\max} = k/k_{\max}$, with $k_{\max} = n-1-|m|$. As expected, states of k and $-k$ give symmetrical profiles with respect to $k'=0$.

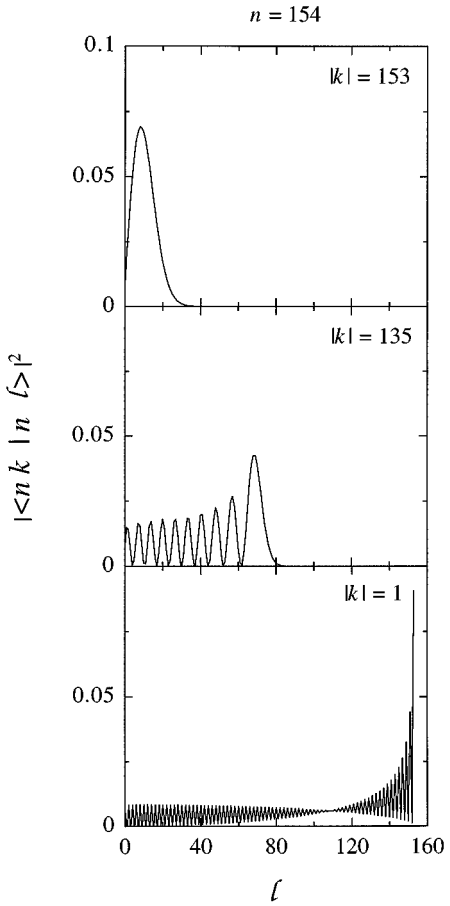

FIG. 5. Weights $|\langle nk|nl\rangle|^2$ of the parabolic states $|k|=153,135,1$ ($m=0$) as a function of the zeroth-order l states for $n=154$ [Eq. (7)]. The highest parabolic state $|k|=153$ (upper panel) is the most localized in l and is spread over the region in l for which the coupling strength in the hydrogenic basis is maximum (cf. Fig. 1). The state $|k|=135$ (middle panel) covers the full range of the dipolar coupling (up to $l/n=0.7$). The lowest parabolic state $|k|=1$ (lower panel) is the most delocalized in l and has the largest weights in the region $l/n \geqslant 0.7$.

As can be seen from Fig. 6, there is a correlation between the l content of the parabolic state and the strength of dipolar the coupling: parabolic states essentially localized in l larger than l_0 (≈ 80) have a significantly smaller coupling (by an order of magnitude) than parabolic states localized in low l. This correlation can be understood by looking at how diluted the coupling strength of an n Stark state of a given k is with respect to the zeroth-order quantum number l of the hydrogenic n' states. The relevant matrix elements for this purpose are

$$\langle nkm|r^{-2}|n'lm'\rangle = \sum_{l'=0}^{n-1} \langle nkm|nl'm\rangle \langle nl'm|r^{-2}|n'lm'\rangle,$$

$$\delta_{ll'} = \pm 1, \quad \delta_{mm'} = 0. \tag{9}$$

These dipolar matrix elements [Eq. (9)] for the three parabolic states plotted in Figs. 5 and 6 ($n=154$, $|k|=153,135,1$, and $n'=113$) are plotted in Fig. 7 as a function of l. Their behavior with respect to l can be predicted from the behavior

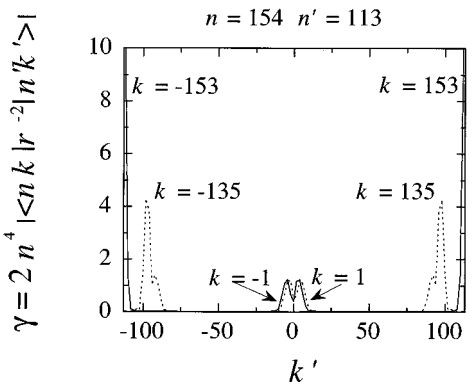

FIG. 6. Dipolar matrix elements $|\langle nk|r^{-2}|n'k'\rangle|$ [Eq. (8)] between parabolic states $n=154$, $|k|=153,135$, 1, and $n'=113$ as a function of k'. The matrix elements of a given k value are well localized in k' around a value k'_m approximately given by $k'_m/k'_{\max}=k/k_{\max}$, with $k_{\max}=n-1-|m|$. The matrix elements are shown multiplied by n^4, the density of states in a given Rydberg series in the presence of an external field, as in Figs. 2 and 3.

of the hydrogenic radial matrix elements $\langle nl|r^{-2}|n'l\pm1\rangle$ (Fig. 1) and the l content of the $n=154$ $|k|$ states plotted in Fig. 5. When the range of the $|k|$ state in l is smaller than l_0 ($\approx$80), the range of the dipolar matrix element $\langle nk|r^{-2}|n'l\rangle$ in l is governed by the range of the $|k|$ state (Fig. 7, upper panel) and the coupling strength is large. On the other hand, when the extension of the $|k|$ state in l is larger than $l_0\approx80$, the range of the dipolar matrix element $\langle nk|r^{-2}|n'l\rangle$ in l is limited by l_0 (middle and lower panels of Fig. 7), so that the coupling is significantly smaller. Parabolic states $-k$ and k have the same absolute value $|\langle nk|r^{-2}|n'l\rangle|$. Their amplitudes differ by a sign.

In Fig. 8, the dipolar matrix elements $|\langle nk|r^{-2}|n'k'\rangle|$ are plotted as a function of $|k|$ for two values of n', $n'=140$ and 113. The chosen value of k' is that which corresponds to the largest magnitude of the matrix element (cf. Fig. 6). Lower-$|k|$ states, mostly localized in the range $l\geqslant l_0$, have a lower coupling strength. In agreement with Fig. 9 below, a larger value of n' corresponds to a smaller dipolar coupling strength. What also appears from Fig. 8 is that, due to the long range of the dipolar interaction, there is no significant dilution of the dipolar coupling strength induced by the field. Of course, all the parabolic states get some coupling strength, while in the hydrogenic states basis, only states up to $l/\min(n,n')\simeq0.5$ (where n is small) are coupled. However, by comparing Fig. 8 with Figs. 2 and 3, it can be seen that the average coupling strength is of the same order of magnitude in the l or in the k basis set. This is unlike the case of the quadrupolar interaction, which is localized in low-l values in hydrogenic states (for the quadrupolar interaction, l_0 is about 10). In parabolic states, the average coupling strength of a quadrupolar term indeed is reduced, by approximately a factor $1/n$ on the average, because of the dilution due to l mixing.

To conclude this section, we show that significant coupling persists at large Δn in parabolic states too. This is illustrated in Fig. 9, where the dipolar matrix elements $|\langle nk|r^{-2}|n'k'\rangle|$ for the parabolic states $n=154$ and $|k|=153,135,1$, plotted as a function of n', are seen to increase with Δn. This monotonic increase is due to the mixing of the

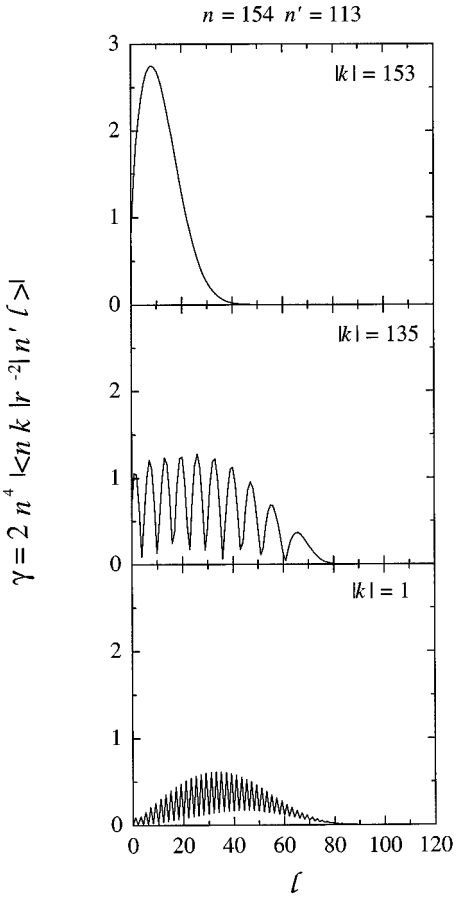

FIG. 7. Dipolar matrix elements between parabolic states $n=154$ and $|k|=153,135$, 1, and hydrogenic states $n'=113$ as a function of l [Eq. (9)]. In the upper panel, the extent of significant dipolar coupling is governed by the l range of the high-$|k|$ state (cf. Fig. 5, upper panel), while for the lower $|k|$ states of the middle and lower panels, it is governed by the range of the dipolar coupling in the nl basis set (cf. Fig. 1). As in Figs. 2, 3, and 6, the matrix elements are shown multiplied by $\rho=n^4$, the density of states of a given Rydberg series in the presence of an external dc field.

hydrogenic l states, for which the dipolar coupling reaches higher magnitudes and occurs at lower-n' values for lower values of l (see Fig. 3). From Eq. (8), it can be seen that the orthogonality relation for $\Delta n=0$ (which is not clearly seen because of the logarithmic scale) remains valid for the parabolic states. Note that parabolic states used in this section are a zeroth-order description in that they take only the l mixing into account. Above the Inglis-Teller limit, the intraseries n mixing due to the field (which is included in Fig. 12 and in the dynamical computations presented in Sec. VI below) leads to a more uniform distribution of the coupling strength.

V. INTERSERIES DIPOLAR COUPLING

We discuss, for simplicity, two series of bound Rydberg states, built on different rotational states of the core and coupled by the dipolar interaction. The difference in rotational energy means that in a given band of quasi-isoenergetic zeroth-order states one series is denser than the other, where the zeroth-order Hamiltonian is $H_0+H_{\rm rot}$ [cf. Eq. (5)]. In the presence of an external dc field, we add to the

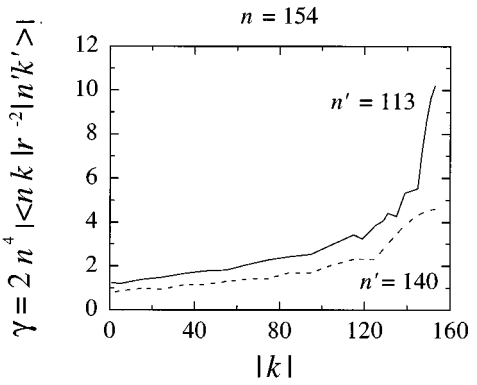

FIG. 8. Variation of the dipolar matrix elements $|\langle nk|r^{-2}|n'k'\rangle|$ as a function of k for $n=154$ and $n'=140$ (dashes) and 113 (full lines). As shown in Fig. 10 below, these values of n' correspond to isoenergetic states in the Rydberg series built upon the $j=1$ rotational states of the core for rotational constants of $B=0.48$ and 1.9842 cm^{-1}, respectively. The latter is the value for NO^+. The value of k' corresponds to the largest matrix element (see Fig. 6) and varies with n'. The matrix elements are multiplied by n^4, the density of states in a given Rydberg series in the presence of an external dc field. The strength of the coupling increases with Δn (see Fig. 9 below). By comparing with Fig. 2 for the matrix elements $n=154$ and $n'=113$, it can be seen that there is no dilution of the coupling strength due to the external dc field. The value of $\gamma=2V\rho$ is of the same order of magnitude in the l and in the k basis.

Hamiltonian of Eq. (5) the intraseries Stark coupling (leading to both l and n mixing).

For two series of Rydberg states there are three energetic parameters, say, the interseries coupling V and the density of states in the two series $\delta E(i)$, $i=1,2$. The extent of the interseries coupling is, on the average, characterized therefore by the magnitude of two dimensionless coupling parameters. These can be taken to be $\gamma_i=2V/\delta E(i)$ [58].

The strong coupling limit is $\gamma>1$, whereas the sparse coupling limit is the opposite. The reason is that, as in other areas of dynamics, γ_i is the mean number of states of series i that are within the range of the coupling of a state in the other series. Since n is high it is typically the case that $\gamma_1>\gamma_2$ is the most common situation below the threshold for rotational autoionization and in the presence of a dc field one has $\gamma_1>1>\gamma_2$. Under such circumstances the transfer of population in one direction is effective but much less so in the other direction.

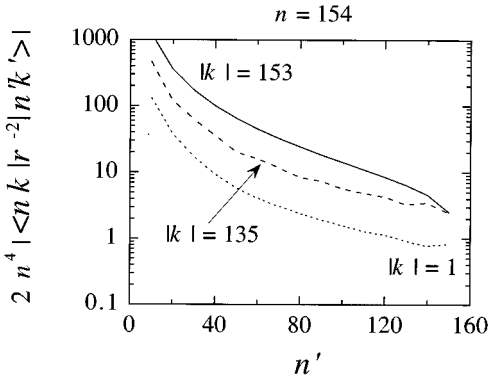

FIG. 9. Dipolar matrix elements (multiplied by n^4) for a given k and $n=154$ as a function of n' on a $\log_{10}$ scale. The chosen value of k' corresponds to the largest matrix element (see Fig. 6) and varies with n'. For $n'=154$, the matrix elements are zero, in agreement with the orthogonality relation. Significant coupling strength is obtained for the whole range of Δn values.

So far we have discussed the average behavior that is expected when the density of states varies essentially smoothly and continuously. That is, however, not necessarily the case when the electrical field is so weak that for one (or both) series the Stark manifolds of adjacent Rydberg states do not overlap.

The key role of the field for interseries coupling is due to the dependence of the coupling parameter on the density of states. In the absence of a dc field, most states of given n are essentially degenerate, except for those of lowest l's, which are split by the quantum defect. There are therefore gaps in the distribution of states in energy and on the average it is unlikely to find a state of the other series within the coupling range $2V$ of a state of the first series. Once the field is above the Inglis-Teller limit the states are about uniformly spread in energy. (While a further increase of the field will push states of a given n farther apart, states of $\Delta n=\pm 1$ will move into the energy range [cf. Fig. 4(b)] so that the density of Rydberg states will not change significantly [59].) We thus have that $\delta E(i)$ in a.u.$=n^{-3}$ for an isolated molecule or n^{-4} in the presence of a field above the Inglis-Teller limit [60]. The resulting increase in the coupling strength is, at high n's, of two orders of magnitude. Note also that the onset of this strong coupling is already at rather weak fields $F(\mathrm{V/cm})=1.714\times 10^9/n^5$. When several Rydberg series are coupled, the values of n within a given energy band rapidly declines as j increases. (Recall that two isoenergetic states of adjacent series differ in energy by $2Bj'$.) Eventually one will reach a series that is below the Inglis-Teller limit. The detailed discussion given in connection with Figs. 13, 15, and 17 below is then needed.

In the presence of a field the zeroth-order states of given l will be (Stark) mixed as discussed in Sec. IV. For a more localized electron-core coupling, this will dilute V by a factor proportional to $1/n$, which will about cancel the increase in the density of coupled states. However, and as already noted in Secs. II (cf. Fig. 1) and IV, for a dipolar coupling the dependence of the coupling matrix element on l is qualitatively different so that the primary role of the field is to increase the coupling parameter due to its influence on the density of states.

The magnitude of the interseries coupling is quite sensitive to the magnitude of the rotational constant B of the core and to the rotational state. Figure 10 shows that value of n' that is degenerate with a given value of n, for the two series $j-1$ and j,

$$n'^{-2}=n^{-2}-4B(\mathrm{a.u.})j.$$

Effective interseries coupling requires (cf. Figs. 3 and 9) that the change in n is large compared to 1. Hence one needs that $1\ll\Delta n\approx 4Bjn^3<n$ or, using the condition that strong coupling requires $V/\delta E>1$,

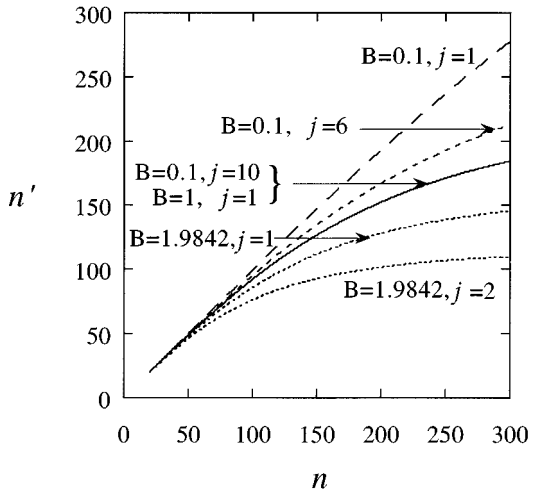

FIG. 10. Value of n' of the Rydberg state in the series built on j that is about isoenergetic with a state n of the series $j-1$ vs n. The results are shown for different values of the rotational constant B (in cm^{-1}) and for different values of j. The energy difference between the two series is $2Bj$ and if this is too small, Δn is not large and the coupling (cf. Fig. 3) is not large. See also Fig. 6.

$$(4Bj/Vn)>1 \tag{10}$$

for strong coupling in the presence of a field.

The discussion so far has emphasized on the average behavior. Particularly in the sparse coupling limit $\gamma<1$, where the density of states is very nonuniform, there can be considerable local variations in the interseries energy spacing (or ''detuning'') from one state to the next one of the same series. Figure 11 provides a graphical demonstration of this point. Shown is the spacing, for consecutive states of a given series, between the state to the state nearest in energy of the *other* series. To emphasize the wide local variations, the detunings are plotted on a logarithmic scale. Effective local coupling requires that $2V$ be large compared to these detunings. The order of magnitude of the radial matrix element (in a.u.) is less than 8. Hence, in the absence of a field, unless the dipole moment is large compared to 1 a.u., it is typically the case that only every so often is the local coupling effective. On the average, it is not. Figure 11 shows the detunings in the absence of a field so the conclusion that the coupling is occasionally effective but otherwise is not is consistent with the coupling being, on the average, weak. It requires a field to reduce the detunings. When the field is above the Inglis-Teller limit of both series, the average is also the local behavior.

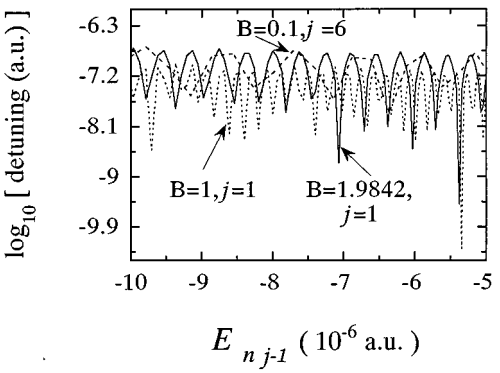

FIG. 11. Small energy difference (the detuning is in a.u. on a $\log_{10}$ scale) between two nearly isoenergetic Rydberg states that belong to two adjacent Rydberg series vs the energy ($\times 10^6$/a.u.) in the lower series $-(1/2n^2)+B$(a.u.) $(j-1)j$, shown for three values of B (in cm^{-1}) and j (cf. Fig. 10). These detunings will be closed in the presence of a dc field, but in its absence the dipolar coupling (Figs. 1–3) needs to overcome the energy mismatch if the coupling is to be effective.

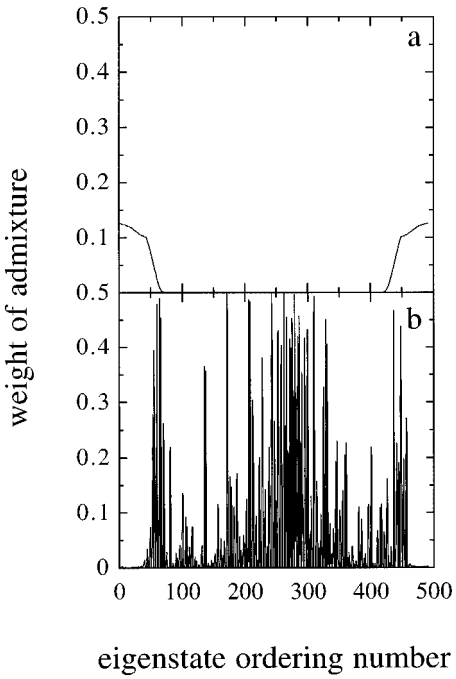

FIG. 12. Interseries coupling of two Rydberg series ($n=154$, $j=0$ and $n=113$, $j=1$) in the (a) absence and (b) presence of a dc field (0.0197 V/cm, which is the Inglis-Teller onset for $n=154$). The wave functions are determined by diagonalization of the Hamiltonian in the subspace $M=0$. Shown is the weight of the zeroth-order state of the ''other'' series for the different eigenstates arranged in order of increasing energy.

Figure 11 also shows the importance of the condition (10). The bigger the value of $2Bj$, the more common the occurrence of low detunings. We reiterate that Fig. 11 is a ''worst case'' scenario as it is in the absence of a field.

The local variations in the effective interseries coupling are reflected in the nature of the wave function. Plotted in Fig. 12 are the weight of the zeroth-order state of a given j in the other series. In the absence of the field, when the coupling is weak, the coupling is quite regular and occurs only when there is a near degeneracy of the two series. Once a field is present, the variation is more extreme and occurs throughout [61,62]. The details of the computations in Fig. 12 are those of Fig. 15 below.

VI. DYNAMICS

The Hamiltonian (5) with, in addition, the intraseries l and n coupling matrix elements due to an external dc electric field was numerically diagonalized, using the conservation of M to reduce the size of the matrix. Thereby the survival

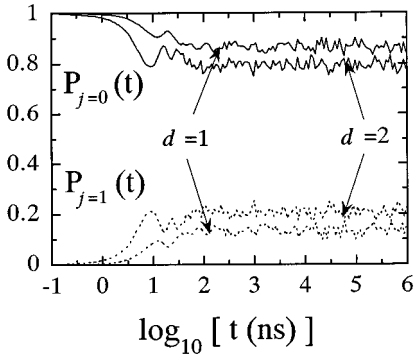

FIG. 13. Time evolution for the initial state $n=125$ and $l=1$ of the $j=0$ series shown vs time in nanoseconds on a $\log_{10}$ scale. $P_j(t)$ is the population in all the zeroth-order states of the jth series. The higher the dipole d, the more extensive the transfer.

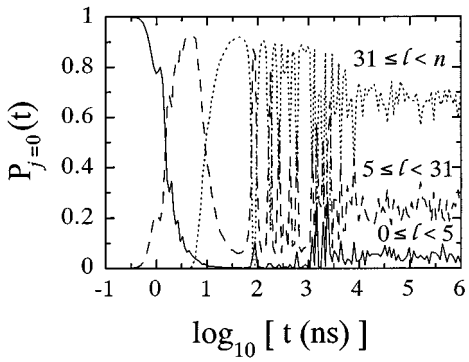

FIG. 14. Population in different groups of states all of $j=0$ and $n=154$, but with different ranges of l, as indicated for an initial state $j=0$, $n=154$, and $l=2$ plotted vs time in nanoseconds on a $\log_{10}$ scale. The transfer to the $j=1$ series is allowed for, yet by 10^4 ns the populations have reached a steady state reflecting the number of quantum states in each group.

probability of the initial state $|C(t)|^2 \equiv |\langle\psi(0)|\psi(t)\rangle|^2 = \langle\psi(t)|Q|\psi(t)\rangle$, where Q is a projection on the initial state, and also the occupation probability $P(t)$ of any other state φ_i, $P_i(t)=|\langle\varphi_i|\psi(t)\rangle|^2=\langle\psi(t)|\varphi_i\rangle\langle\varphi_i|\psi(t)\rangle$, or group of states $P(t)=\Sigma_i P_i(t)$ can be evaluated. The computations were at an energy below the threshold for rotational autoionization so that only discrete-discrete interseries coupling is possible [63–65]. Even so, when the coupling is effective the interseries coupling can be defacto dissipative [66,67].

Figure 13 compares the transfer between two series for two values of the dipole of the core ($d=1$ and 2 a.u.) for a field (0.056 V/cm) that is above the Inglis-Teller limit for both series. $B=1.9842$ cm^{-1}. The initial state is $n=125$, $j=0$, and $l=1$ and the figure shows the occupation of all zeroth-order states of $j=0$ and of a nearly isoenergetic set of states $n=100$ and $j=1$ in the other series. The computation is for $M=0$. Note that there are more states of $j=1$ because for $M=0$ all values of m_j are accessible. The transfer is complete on a time scale of about 100 ns, which is comparable to the minimal time delay that is usually possible in ZEKE experiments [68]. At energies above threshold for rotational autoionization, a population transfer of 10–20 % to lower n's will amply suffice to provide a long-time component as observed in typical ZEKE experiments.

At longer times the evolution is essentially dissipative. We provide several backups for this claim. First consider the intraseries dynamics (Fig. 14). Shown is the population in different groups of $j=0$ states, classified according to the value of l. As expected from the breadth of the Stark splitting (1.36×10^{-7} a.u. or a period of 33 ns for $n=154$ and $F=0.0197$ V/cm, 1 a.u.$=5.142\times10^9$ V/cm) by approximately 10 μs, the population in the $j=0$ series is about uniform in the sense that the population in a group of states is proportional to the number of states in the group. Next, consider two different initial states, one in the $j=0$ series as in Fig. 9 ($n=154$, $j=0$, and $l=0$) and the other in the $j=1$ series ($n=113$, $j=1$, and $l=0$). Since the density of states is higher in the $j=1$ series (because of the extra degeneracy of the rotational states), the transfer is more extensive in the $j=0\rightarrow j=1$ direction (Fig. 15). By about 300 ns (for a dipole of 1 a.u.) the distribution of populations among the two series has reached a steady state. Note that comparing Figs. 14 and 15, the interseries coupling reaches a plateau first.

The time evolution seen in Fig. 13–15 is modulated. To show that this is due to Stark oscillations [69], a linear time scale is used in Fig. 16. Unlike the case of localized coupling, here the Stark modulation of l does not quench the coupling, but does cause it to vary with the Stark period. Of course, the oscillations are possible because l is not a good quantum number in the presence of a field and the zeroth-order states are chosen to be hydrogenic (i.e., of given l). Because in the linear Stark regime the splittings of the states are equidistant, there is a correspondence between the classical description where l is modulated by the Stark frequency [41] and the quantum-mechanical time evolution.

A point that was checked is the role of l. The results shown in Fig. 12(b) were repeated, but when coupling was allowed only for states with $l>4$. This had hardly any effect. In Fig. 13 the time evolution was recomputed when all states of $l\leqslant4$ were assigned a zero interseries coupling. This had a negligible effect. The results shown in Figs. 12–16 are all for $M=0$. The computations were repeated for higher values of M so as to verify that there are no essential changes. This is to be expected because increasing the value of M cuts the lowest value of l that can contribute. These results suggest

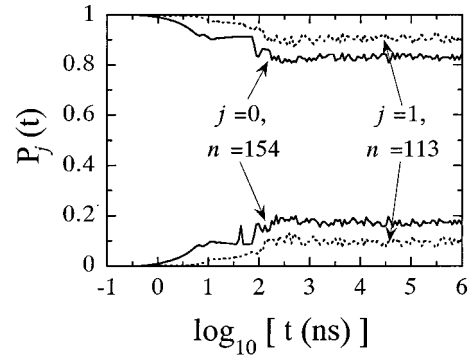

FIG. 15. Time evolution for two different initial states in the $j=0$ and 1 series, respectively, shown vs time in nanoseconds on a $\log_{10}$ scale. Initially $l=0$. The transfer is more extensive in the $j=0$ to $j=1$ direction because there are more nearly isoenergetic quantum states in the $j=1$ series.

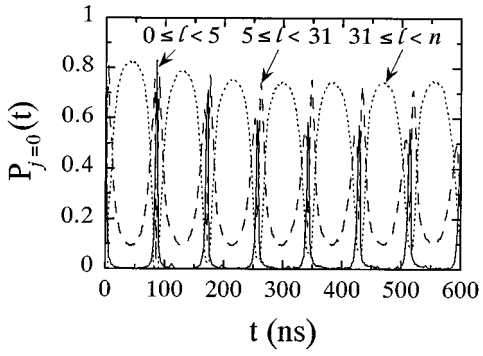

FIG. 16. Time evolution for an initial state in the $j=0$ series shown vs time in nanoseconds on a linear scale. Same conditions as in Fig. 9. Shown are the populations of three different groups of states in the $j=0$ series, where the states are classified according to their value of l, as indicated. The Stark oscillations are clearly evident.

that even higher M states are not immune to interseries coupling. This should be detectable by means of rotational state-selective pulsed field ionization.

The role of the dc electric field is shown in Fig. 17. The computation uses states with several adjacent values of n in the $j=0$ series and a somewhat higher field (0.1 V/cm) so that both the $j=0$ and 1 series are above the Inglis-Teller limit. $B=1.9842\ \mathrm{cm}^{-1}$. Shown are the populations in the two series for initial states of $n=154$, which in the absence of a field are nearly isoenergetic with $n=113$ of the $j=1$ series and for $n=153$, which in the absence of a field is quite detuned from states of the $j=1$ series. The initial states used differ also in the value of l ($l=0,1,2,3$). It is evident that when the field is above the Inglis-Teller limit for both series the coupling is evenly spread and that the local variations have been smoothed.

VII. CONCLUDING REMARKS

The coupling of the Rydberg electron to a dipolar molecular core was found to be important, particularly so at times much longer than the orbital period of the electron. Due to the long-range nature of the interaction, the coupling affects also states of higher orbital angular momentum, up to $l/n \approx 0.5$ (see Fig. 1 and the Appendix). Therefore, the presence of a weak dc field does not dilute the strength of this coupling. Indeed, for a dc field above the Inglis-Teller limit [$3n^5F$ (a.u.)>1] the field acts so as to provide a smooth density of states, thereby ensuring that coupling of Rydberg series associated with different states of the core occurs throughout and is not limited to accidental resonances. The long-range nature of the anisotropic coupling means that Rydberg states of very different n's can strongly interact (Figs. 2, 3, 8, and 9) and this too favors interseries coupling. Methodologically, the long-range nature of the coupling requires that realistic computational studies include states of high l of the different Rydberg series. The long times needed for the population to uniformly sample the available phase space (Figs. 13–15 and 17) means that the role of the dipolar coupling is more readily experimentally explored in the time domain rather than spectroscopically.

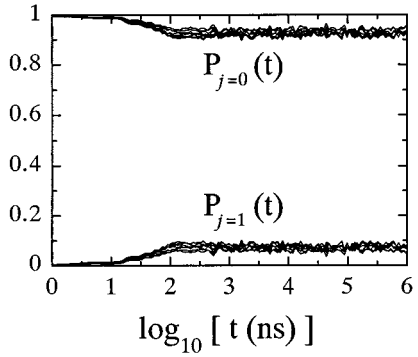

FIG. 17. Time evolution when the dc electric field is above the Inglis-Teller limit for both series (time is in nanoseconds on a $\log_{10}$ scale). For six different initial states, with small and large detunings, the time evolution is essentially the same.

ACKNOWLEDGMENTS

We thank H.-J. Dietrich, A. Held, J. Jortner, E. W. Schlag, A. Stolow, U. Even, M. Vrakking, and B. Zon for discussions and comments. This work was supported by SFB 377 and by the German-Israel James Franck Binational Program. F.R. is a Chercheur Qualifié of FNRS, Belgium.

APPENDIX: NUMERICAL COMPUTATION OF RADIAL MATRIX ELEMENTS IN A HYDROGENIC BASIS

1. Definitions

The following convention [31] on the form of the radial wave functions of bound hydrogeniclike states in a coordinate representation is used:

$$S_{\nu\lambda}(r)\equiv rR_{\nu\lambda}(r)=\frac{1}{a^{1/2}\nu}\left(\frac{n_r!}{\Gamma(\nu+\lambda+1)}\right)^{1/2}\left(\frac{2r}{a\nu}\right)^{\lambda+1}L_{n_r}^{(2\lambda+1)}\times\left(\frac{2r}{a\nu}\right)\exp\left(-\frac{r}{a\nu}\right), \tag{A1}$$

where λ is a real number $\lambda>-\frac{1}{2}$; ν is the ''principal'' quantum number $\nu=n_r+\lambda+1$, which need not be an integer; n_r (a non-negative integer) is the radial quantum number, which is equal to the number of nodes in $R_{\nu\lambda}(r)$. $a=\hbar^2/\mu Ze^2$, where μ is the reduced mass and Z is the charge on the core. In atomic units and for the case of singly charged core $\hbar=e=Z=1$ and $\mu\approx 1$. $L_N^{(\alpha)}(x)$ is the generalized Laguerre polynomial

$$L_N^{(\alpha)}(x)=\sum_{m=0}^{N}\frac{(-1)^m}{m!}\binom{N+\alpha}{N-m}x^m. \tag{A2}$$

The radial wave functions as defined above are orthonormal

$$\int_0^\infty dr\ S_{\nu'\lambda}(r)S_{\nu\lambda}(r)=\delta_{\nu'\nu}\quad\text{if}\quad \nu'-\nu=0(\mathrm{mod}\ 1) \tag{A3}$$

and are solutions of the radial Schrödinger equation

$$\left(-\frac{\hbar^2}{2\mu}\frac{d^2}{dr^2}+\frac{\lambda(\lambda+1)}{2\mu r^2}-\frac{Ze^2}{r}+\frac{\mu Z^2e^4}{2\hbar^2\nu^2}\right)S_{\nu\lambda}(r)=0. \tag{A4}$$

For integer values of $\lambda=l$ and $\nu=n$, $S_{nl}(r)$ are hydrogenic radial wave function, l being the angular momentum. At a general noninteger λ, $S_{\nu\lambda}(r)$ are the radial wave functions that appear, for instance, within the framework of the model of Rydberg states in the presence of a dipole [49–51] and are sometimes interpreted as hydrogeniclike states with a quantum defect $\delta=l-\lambda$, l being the nearest integer to λ.

The identity (4) is derived by using both (A4) and the corresponding radial equation for $S_{\nu'\lambda'}(r)$. Premultiplying (A4) by $S_{\nu'\lambda'}(r)$ and integrating over r yields the desired result when the definition (A5) below is used.

2. Computation of radial elements

Radial matrix elements of an operator diagonal in coordinate representation are defined as usual by

$$\langle\nu'\lambda'|f(r)|\nu\lambda\rangle=\int_0^\infty dr\; S_{\nu'\lambda'}(r)f(r)S_{\nu\lambda}(r). \tag{A5}$$

For computations requiring a large number of matrix elements and when an accuracy of about 1% is sufficient, the method due to Zimmerman *et al.* [27,30] is sufficient, particularly if l is below $n/2$. This method is based on the Numerov integration of the radial Schrödinger equation combined with a simple form of numerical quadrature. For high values of n and particularly if l is also high, the Numerov method calls for additional care or another method is needed.

The method we propose is more expensive in computer time but provides a far higher accuracy. The method is based on the reliable computation of the generalized Laguerre polynomials, which are used in (A1) so that the evaluation of the radial matrix elements is done via (A4) using quadrature. The method is based on the recurrence relations for generalized Laguerre polynomials (equation 22.7.12 of Ref. [70])

$$\begin{aligned} L_0^{(2\lambda+1)}(x)&=1,\\ L_1^{(2\lambda+1)}(x)&=2(\lambda+1)-x,\\ L_N^{(2\lambda+1)}(x)&=\{[2(N+\lambda)-x]L_{N-1}^{(2\lambda+1)}(x)\\ &\quad-(N+2\lambda)L_{N-2}^{(2\lambda+1)}(x)\}/N \end{aligned} \tag{A6}$$

and we present two variants, depending on how these relations are used to generate the polynomials. The closed form (A2) cannot be used for computer calculation of Laguerre polynomial of high orders N because successive terms alternate in sign. Straightforward summation of the power series (A2) on a machine with a finite relative precision (double precision $\varepsilon_{\text{machine}}=2^{-52}=2.2\times10^{-16}$) results in excessive roundoff noise due to numerical cancellation of individual terms. Already for $n=100$ and $l=0$, the noise is 31 orders of magnitude larger than the accurate result.

The first variant is to compute the Laguerre polynomials with high accuracy directly using the recurrence relations (A6). The second variant combines the recurrence relations with the multiplicative form of Laguerre polynomials

$$L_N^{(2\lambda+1)}(x)=\frac{(-1)^N}{N!}\prod_{i=1}^{N}(x-r_i^{(N-\lambda)}), \tag{A7}$$

$r_i^{N\lambda}$ being the ith root of the polynomial $L_N^{(2\lambda+1)}(x)$. This form does not suffer from numerical cancellation of errors and provides the best possible numerical accuracy.

Golub [71] noted that the roots of classical orthogonal polynomials are eigenvalues of the corresponding recurrence relations. After renormalization of the generalized Laguerre polynomials

$$P_N=\binom{N+2\lambda+1}{N}^{-1/2}L_N^{(2\lambda+1)} \tag{A8}$$

and with following definitions of column vectors p,t and symmetric tridiagonal $N\times N$ matrix $A^{(N\lambda)}$: $p=\text{col}[P_0(x),P_1(x),\ldots,P_{N-1}(x)]$, $t=\text{col}[0,0,\ldots,a_{N-1N}P_N(x)]$, and $(A^{(N\lambda)})_{NM}\equiv a^{NM}$, the recurrence relations (A6) can be recast in the matrix form

$$\begin{aligned} a_{NN}&=2(N+\lambda+1),\\ a_{NN-1}&=a_{N-1N}=-[N(N+2\lambda+1)]^{1/2},\\ A^{(N\lambda)}p+t&=xp. \end{aligned} \tag{A9}$$

If x is a root of $P_N(x)$, $x=r_i^{N\lambda}$, then $t=\text{col}(0,0,\ldots,0)$ and Eq. (A9) takes the form of the matrix eigenvalue problem, with $r_i^{N\lambda}$ being eigenvalues of the symmetric tridiagonal matrix $A^{(N\lambda)}$. Hence the roots $r_i^{N\lambda}$ of $L_N^{(2\lambda+1)}(x)$ can be determined very accurately by employing stable procedures for diagonalization, such as imtql2 of EISPACK [72]. Given the necessity of generating the wave function on a dense grid, the diagonalization step does not appreciably increases the cost of the computation.

In order to obtain accurate matrix elements, the accuracy of the numerical wave function should be matched by the accuracy of the numerical quadrature. We used for this purpose the adaptive procedures dqdag and dqdagi from the IMSL standard library, which are based on the Gauss-Kronrod rules, enabling automatic adjustment to within the required tolerance.

The accuracy of the matrix elements obtained by the two variants was checked by comparing the value of the left-hand side and the right-hand side of the identity given in Eq. (1) at integer values of l and l' and by computation of the identity (4) at integer and noninteger values of l and l'. The orthonormalization conditions (A3) and the known diagonal elements [31,73] provide additional and complementary tests for accuracy. Such tests were conducted over a wide range of values of ν, ν', λ, and λ': $\frac{1}{2}<\nu$, $\nu'\leq500$, $-\frac{1}{2}<\lambda\leq\nu-1$, and $-\frac{1}{2}<\lambda'\leq\nu'-1$ for $f(r)=r^k$, $k=-3,-2,0,1,2$. These tests indicate that the relative accuracy of the matrix elements was typically better than 10^{-14} and in all the tests was better than 10^{-12}. The higher accuracy is expected for the second variant, based on (A9). At the high n's of interest and for $l<n$ the accuracy of the fast Numerov method due to Zimmerman *et al.* [27] was found to be of the order of 1%.

3. Limitations of the near-threshold approximation for the radial wave functions

For states just below the threshold for ionization it is suggestive to use the Bessel function approximation [31] for the radial wave functions. This is particularly convenient for such cases as a dipolar coupling where the integration of (A6) is analytic. Unfortunately, as will now be discussed, the method is not accurate for dipolar coupling at any but the lowest l's.

The near-threshold approximation is valid for weakly bound states when attention is centered on low values of r. It is then possible to use the approximation

$$\nu^{3/2}S_{\nu\lambda}(r)\rightarrow(2/r)^{1/2}J_{2\lambda+1}[(8r)^{1/2}], \qquad \text{(A10)}$$

valid for $\nu\rightarrow\infty$, while r and λ are finite. It is important to note that the Bessel function approximation (A10) is the first term in a convergent series expansion and that higher terms in the series can be obtained using equations 22.5.4 and 13.3.7 of Ref. [70]. The reason for making this point is that radial matrix elements computed using (A10) can vanish identically, whereas the exact results do not. When this happens it simply means that the next term in the expansion is not a correction, but the leading contribution to the matrix element.

Using the near-threshold Bessel function approximation (A10) in (A5) leads to an analytical expression for the dipolar coupling [48]

$$\langle\nu'\lambda'|r^{-2}|\nu\lambda\rangle\approx\frac{2}{\nu^{3/2}\nu'^{3/2}(\lambda+\lambda'+1)}\frac{\sin[\pi(\lambda-\lambda')]}{\pi(\lambda-\lambda')}. \qquad \text{(A11)}$$

The most striking aspect of this result is that if $\lambda-\lambda'(\mathrm{mod}1)$ is quite small compared to unity then the matrix element is negligible. The condition is quite common for all Rydberg states but those of lowest l's because at higher l's the quantum defect is very small so that $l\approx\lambda$ and the transitions of interest are those of $|\Delta l|=1$. In fact (see Fig. 18), the exact matrix element does not vanish. Rather, the leading contribution is made by the next term neglected in (A10).

Figure 18 provides a comparison between the exact results (solid line) and the approximation (A11) (dashed line) for a low and an intermediate value of λ for $n=154$ and $n'=113$. It is seen that when λ/n is not small compared to unity, the error is considerable. Most of the coupling terms of importance in the Hamiltonian fall in this range. Note also that in both panels of Fig. 18, the error is worst in the range of interest, i.e., when $\lambda-\lambda'(\mathrm{mod}1)$ is quite small compared to unity and that even when λ is small, the absolute error in the range of interest is comparable to the average strength of the coupling.

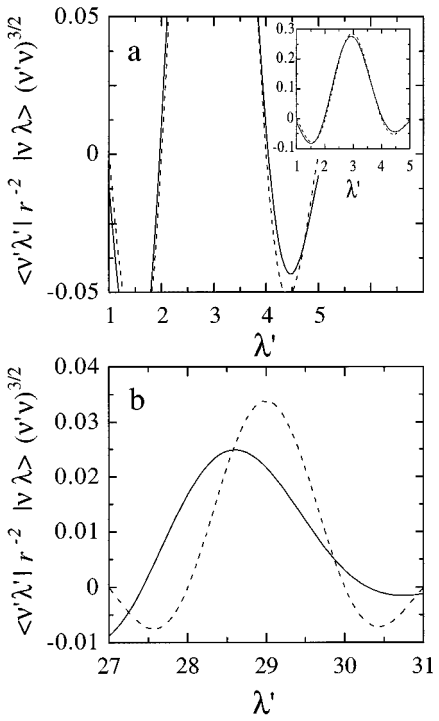

FIG. 18. Dipolar coupling matrix element ($n=154$) plotted against the (effective) final angular momentum λ' for (a) $\lambda=3$ and (b) $\lambda=29$. Solid line, precise numerical integration; dashed line, the analytical approximation (A11) obtained using the near-threshold Bessel function approximation for the radial wave functions. The important matrix elements are those where $\lambda-\lambda'$ (mod1) is quite small compared to unity. This region is emphasized in (a), whereas the inset shows the full range.

By plotting the integrand of (A3) one can see that the shortcoming of the approximation (A11) is due to the long-range nature of the coupling. The exact wave function is phase shifted with respect to the Bessel function. For a coupling with a long range this leads to an accumulation of the error. Moreover, since the phase of the exact wave function varies with the energy and with λ, the error is not constant. The near-threshold approximation is more satisfactory for short-range coupling. In the present problem it correctly accounts for the role of the quantum defects at $\lambda\ll n$ when $\lambda-\lambda'(\mathrm{mod}1)$ is not small.

[1] K. Müller-Dethlefs and E. W. Schlag, Annu. Rev. Phys. Chem. **42**, 109 (1991).
[2] K. Müller-Dethlefs, E. W. Schlag, E. R. Grant, K. Wang, and V. McKoy, Adv. Chem. Phys. **90**, 1 (1995).
[3] K. Müller-Dethlefs, O. Dopfer, and T. G. Wright, Chem. Rev. **94**, 1845 (1994).
[4] R. Linder, H. J. Dietrich, and K. Müller-Dethlefs, Chem. Phys. Lett. **228**, 417 (1994).
[5] L. Zhu and P. Johnson, J. Chem. Phys. **94**, 5769 (1991).
[6] H.-J. Dietrich, R. Lindner, and K. Müller-Dethlefs, J. Chem. Phys. **101**, 3399 (1994).
[7] H. J. Neusser and H. Krause, Chem. Rev. **94**, 1829 (1994).
[8] H. J. Dietrich, K. M. Muller-Dethlefs, and L. Y. Baranov, Phys. Rev. Lett. **76**, 3530 (1996).
[9] G. Reiser, W. Habenicht, K. Müller-Dethlefs, and E. W. Schlag, Chem. Phys. Lett. **152**, 119 (1988).

[10] D. Bahatt, U. Even, and R. D. Levine, J. Chem. Phys. **98**, 1744 (1993).
[11] W. G. Scherzer, H. L. Selzle, E. W. Schlag, and R. D. Levine, Phys. Rev. Lett. **72**, 1435 (1994).
[12] M. J. J. Vrakking and Y. T. Lee, J. Chem. Phys. **102**, 8833 (1995).
[13] M. J. J. Vrakking and Y. T. Lee, J. Chem. Phys. **102**, 8818 (1995).
[14] R. D. Levine, Adv. Chem. Phys. (to be published).
[15] W. A. Chupka, J. Chem. Phys. **98**, 4520 (1993).
[16] S. T. Pratt, J. Chem. Phys. **98**, 9241 (1993).
[17] G. I. Nemeth, H. L. Selzle, and E. W. Schlag, Chem. Phys. Lett. **215**, 151 (1993).
[18] A. Mühlpfordt, U. Even, E. Rabani, and R. D. Levine, Phys. Rev. A **51**, 3922 (1995).
[19] F. Merkt and R. N. Zare, J. Chem. Phys. **101**, 3495 (1994).
[20] F. Merkt, R. S. Mackenzie, and T. P. Softley, J. Chem. Phys. **99**, 4213 (1993).
[21] C. E. Alt, W. G. Scherzer, H. L. Selzle, and E. W. Schlag, Chem. Phys. Lett. **224**, 366 (1994).
[22] C. E. Alt, W. G. Scherzer, H. L. Selzle, E. W. Schlag, L. Y. Baranov, and R. D. Levine, J. Phys. Chem. **99**, 1660 (1995).
[23] M. Bixon and J. Jortner, J. Phys. Chem. **99**, 7466 (1995).
[24] X. Zhang, J. M. Smith, and J. L. Knee, J. Chem. Phys. **99**, 3133 (1993).
[25] M. J. J. Vrakking, I. Fischer, D. M. Villeneuve, and A. Stolow, J. Chem. Phys. **103**, 4538 (1995).
[26] M. Bixon and J. Jortner, J. Chem. Phys. **105**, 1363 (1996).
[27] M. L. Zimmerman, M. G. Littman, M. M. Kash, and D. Kleppner, Phys. Rev. A **20**, 2251 (1979).
[28] S. A. Bhatti, C. L. Cromer, and W. E. Cooke, Phys. Rev. A **24**, 161 (1981).
[29] C. Froese, Can. J. Phys. **41**, 1895 (1963).
[30] T. F. Gallagher, *Rydberg Atoms* (Cambridge University Press, Cambridge, 1994).
[31] H. A. Bethe and E. E. Salpeter, *Quantum Mechanics of One- and Two-Electron Atoms* (Plenum-Rosetta, New York, 1977).
[32] J. M. Bradsley, Chem. Phys. Lett. **1**, 229 (1967).
[33] R. S. Berry, J. Chem. Phys. **45**, 1228 (1966).
[34] R. S. Berry and S. E. Nielsen, J. Chem. Phys. **49**, 116 (1968).
[35] A. Russek, M. R. Patterson, and R. L. Becker, Phys. Rev. **167**, 17 (1968).
[36] U. Fano, Phys. Rev. A **2**, 353 (1970).
[37] G. Herzberg and C. Jungen, J. Mol. Spectrosc. **41**, 425 (1972).
[38] E. E. Eyler, Phys. Rev. A **34**, 2881 (1986).
[39] C. Bordas, P. Brevet, M. Broyer, J. Chevaleyre, and P. Labastie, Europhys. Lett. **3**, 789 (1987).
[40] S. M. Jaffe, R. Kachru, N. H. Tran, H. B. V. L. V. D. Heuvell, and T. F. Gallagher, Phys. Rev. A **30**, 1828 (1984).
[41] E. Rabani, L. Y. Baranov, R. D. Levine, and U. Even, Chem. Phys. Lett. **221**, 473 (1994).
[42] The extra power of r causes a quadratically faster decrease of the matrix elements with l, as can be seen from the analytical expression [31] of the radial diagonal matrix elements of r^{-3}.
[43] See Ref. [31], Sec. 60, Eqs. (60.7) and (60.11) in particular.
[44] I. C. Percival and M. J. Seaton, Proc. Cambridge Philos. Soc. A **144**, 654 (1957).
[45] A. M. Arthurs and A. Dalgarno, Proc. R. Soc. London Ser. A **256**, 540 (1960).
[46] R. B. Bernstein, A. Dalgarno, H. Massey, and I. C. Percival, Proc. R. Soc. London Ser. A **274**, 427 (1963).
[47] F. Remacle and R. D. Levine, J. Chem. Phys. **104**, 1399 (1996).
[48] R. D. Gilbert and M. S. Child, Chem. Phys. Lett. **287**, 153 (1991).
[49] B. A. Zon, Phys. Lett. A **203**, 373 (1995).
[50] B. A. Zon, Zh. Eksp. Teor. Fiz. **102**, 36 (1992) [Sov. Phys. JETP **75**, 19 (1992)].
[51] J. K. G. Watson, Mol. Phys. **81**, 277 (1994).
[52] C. R. Mahon, G. R. Janik, and T. F. Gallagher, Phys. Rev. A **41**, 3746 (1990).
[53] The distance of closest approach at high n's is $l(l+1)/2$.
[54] When, for a neutral molecule, additional, dipole bound states are possible [55,56].
[55] H. W. Sarkas, J. H. Hendricks, S. T. Arnold, V. L. Slager, and K. Bowen, J. Chem. Phys **100**, 1884 (1994).
[56] D. M. Cyr, C. G. Bailey, D. Serxner, M. G. Scarton, and M. A. Johnson, J. Chem. Phys. **101**, 10 507 (1994).
[57] L. Y. Baranov, R. Kris, R. D. Levine, and U. Even, J. Chem. Phys. **100**, 186 (1994).
[58] Since the difference between the two-density of states is a function of the rotational constant B of the core, we can use one coupling constant and B.
[59] The only way to further increase the density of accessible states is to break M as a good quantum number by imposition of an external magnetic field [17–19] or by the presence of other ions [12,20,23].
[60] To see the transition from local to average behavior of the coupling constant, consider the density of states within a Stark manifold. Then $\delta E = 3nF$. At the Inglis-Teller limit $\gamma = 2Vn^4$.
[61] The variation in the weight from one eigenstate to another is what one would expect for quantum fluctuations in the strong-coupling limit in the two-series problem [62].
[62] Y. Alhassid and R. D. Levine, Phys. Rev. A **40**, 5277 (1989).
[63] H. Feshbach, Annu. Rev. **19**, 287 (1962).
[64] R. D. Levine, *Quantum Mechanics of Molecular Rate Processes* (Oxford University Press, Oxford, 1969).
[65] This means that the Hamiltonian is symmetric and can be diagonalized by an orthogonal transformation, unlike the situation when the continuum is energetically accessible. One can then use an effective Hamiltonian within the bound subspace [63,64], which needs to be diagonalized in a biorthogonal basis.
[66] M. Bixon and J. Jortner, J. Chem. Phys. **48**, 715 (1968).
[67] J. Jortner and R. D. Levine, Adv. Chem. Phys. **47**, 1 (1981).
[68] This delay is necessary to remove the promptly produced ions.
[69] M. Born, *Mechanics of the Atom* (Blackie, London, 1951).
[70] *Handbook of Mathematical Functions*, edited by M. Abramowitz and I. A. Stegun (Dover, New York, 1972).
[71] G. H. Golub, SIAM Rev. **15**, 318 (1973).
[72] *Matrix Eigensystem Routines—EISPACK Guide*, edited by G. Goos and J. Hartmanis (Springer-Verlag, New York, 1976).
[73] W. Gordon, Ann. Phys. 2, 1031 (Leipzig) (1929).